Available online at www.sciencedirect.com
ScienceDirect
International Journal of Pharmaceutics 331 (2007) 190–196
INTERNATIONAL JOURNAL OF PHARMACEUTICS
www.elsevier.com/locate/ijpharm

Pharmaceutical Nanotechnology

Differential tumor cell targeting of anti-HER2 (Herceptin®) and anti-CD20 (Mabthera®) coupled nanoparticles

A. Cirstoiu-Hapca [a], L. Bossy-Nobs [a], F. Buchegger [b], R. Gurny [a], F. Delie [a,*]

[a] *Department of Pharmaceutics and Biopharmaceutics, School of Pharmaceutical Sciences, University of Geneva, University of Lausanne, 30 Quai Ernest Ansermet, CH-1211 Geneva 4, Switzerland*
[b] *Division of Nuclear Medicine, University Hospital of Geneva, Switzerland*

Received 19 September 2006; received in revised form 22 November 2006; accepted 4 December 2006
Available online 15 December 2006

Abstract

Two types of antibody-labeled nanoparticles (mAb-NPs) were prepared with the aim to achieve specific tumor targeting. Anti-HER2 and anti-CD20 monoclonal antibodies (mAb) were used as model ligands. Small poly(DL-lactic acid) nanoparticles (PLA NPs) with a mean size of about 170 nm were prepared by the salting out method. Thereafter, the coating of PLA NPs with mAbs was performed in two steps. First, thiol groups (–SH) were introduced on the surface of PLA-NPs by a two-step carbodiimide reaction. The number of –SH groups on the surface of NPs increased from 150 to 400 mmol-SH/mol PLA when cystamine concentrations of 25–1518 mol cystamine/mol PLA were used during the thiolation reaction. In the second step, covalent coupling of antibodies to thiolated NPs (NPs-SH) was obtained via a bifunctional cross-linker, *m*-maleimidobenzoyl-*N*-hydroxy-sulfosuccinimide ester (sulfo-MBS). For both mAbs anti-HER2 and anti-CD20, respectively, the number of –SH functions on the NPs had no influence on the amount of mAb coupled to the NPs. Approximately, 295 anti-HER2 and 557 anti-CD20 molecules, respectively, were covalently coupled per nanoparticle. The NPs size after the coupling reactions was about 250 nm. The specific interaction between tumor cells and mAb-NPs was determined by confocal microscopy using two cell lines: SKOV-3 human ovarian cancer cells (overexpressing HER2) and Daudi lymphoma cells (overexpressing CD20). The results showed the selective targeting of mAb-NPs to tumor cells overexpressing the specific antigen. While anti-CD20 labeled NPs (anti-CD20 NPs) bound to and remained at the cellular surface, anti-HER2 labeled NPs (anti-HER2 NPs) were efficiently internalized. The mAb-NPs represent a promising approach to improve the efficacy of NPs in active targeting for cancer therapy while the choice of the antibody-target system defines the fate of the mAb-NPs after their binding to the cells.

Keywords: Cancer therapy; Polymeric nanoparticles; Coated nanoparticles; Active targeting; Monoclonal antibodies; Anti-HER2; Herceptin®; Anti-CD20; Mabthera®

1. Introduction

Major drawbacks of conventional chemotherapy are a modest tumor response and dose limiting side effects due to non-specific biodistribution of drugs. In the last decades, significant progress has been made in development of new delivery technologies. Drug carrier systems emerged as promising approaches in anti-cancer treatment with major advantages: the capacity to improve the therapeutic index of drugs by preferential localization at target sites and lower distribution in healthy tissues, delivery of hydrophobic drugs, high drug loading capacity and controlled release rate (Brigger et al., 2002; Panyam and Labhasetwar, 2003).

Depending on the nanocarrier formulation, drug targeting concepts can be achieved via either passive or active targeting. Tumors are characterized by pathological angiogenesis, leaky vasculature and poor lymphatic drainage, which promote the extravasation and accumulation of macromolecules, a phenomenon known as enhanced permeability and retention (EPR) effect. This phenomenon allows the passive tumor targeting of long-circulating nanocarriers, such as nanoparti-

Abbreviations: NP, nanoparticle; mAb, monoclonal antibody; mAb-NPs, antibody coupled nanoparticles; anti-HER2 NPs, modified NPs with anti-HER2 monoclonal antibody; anti-CD20 NPs, modified NPs with anti-CD20 monoclonal antibody; –SH, thiol groups; PLA, poly(DL-lactic acid); NPs-SH, thiolated nanoparticles; Sulfo-MBS, *m*-maleimidobenzoyl-*N*-hydroxy-sulfosuccinimide ester; CDC, complement-dependent cytotoxicity; ADCC, antibody-dependent cellular cytotoxicity; FDA, United States Food and Drug Administration; MPS, mononuclear phagocytic system; CHOP, combination of cyclophosphamide, doxorubicin, vincristine and prednisone

* Corresponding author. Tel.: +41 22 379 65 73; fax: +41 22 379 65 67.
E-mail address: Florence.delie@pharm.unige.ch (F. Delie).

0378-5173/$ – see front matter © 2006 Elsevier B.V. All rights reserved.
doi:10.1016/j.ijpharm.2006.12.002

cles or liposomes (Duncan, 1999; Maeda, 2001; Brigger et al., 2002).

In a further development, active targeting combines the potential of nanoparticulate systems to carry anticancer drugs with the capacity of the ligand to target specifically malignant cells. More efficient distribution of the drug to tumor tissue, higher efficacy in earlier stages of cancer and higher drug levels in target cells are expected to be reached and maintained for a longer time with this latter approach (Koo et al., 2005).

Active targeting can be achieved by covalent attachment to the surface of nanocarrier systems of different target-specific ligands, such as antibodies or peptides. Different mAb modified immunoliposomes for specific targeting are described in the literature (Park et al., 1997; Sapra and Allen, 2003; Lukyanov et al., 2004). Polymeric nanoparticles represent an attractive approach for specific targeting especially regarding their biocompatibility, biodegradability and stability. Polymers, such as PLA approved by FDA for medical devices are good candidates for drug delivery applications (Ignatius and Claes, 1996). Free carboxylic end groups of PLA offer the possibility of surface modification by introduction of sulfhydryl functions, which allow the covalent coupling of proteins (Nobs et al., 2006).

Among numerous antigens present on malignant cells, HER2 is an interesting target for therapy. Being a member of the epidermal growth factor (EGF) family of receptor tyrosine kinases, HER2 is overexpressed in a variety of human cancers including lung, breast and ovarian carcinomas (Harries and Smith, 2002). Anti-HER2 (trastuzumab, Herceptin®) is a humanized mAb designed to specifically antagonize the HER-2 function. This monoclonal antibody was approved by the FDA in 1998 for treatment of metastatic breast cancer. Many mechanisms have been proposed to explain the therapeutic effect of Herceptin® including internalization and degradation of HER-2, inhibition of angiogenesis and activation of apoptotic signals, but they remain overall controversial (Nahta and Esteva, 2006).

The chimeric anti-CD20 mAb (rituximab, Mabthera®) was approved by the FDA for treatment of non-Hodgkin's B-cell lymphoma in 1997. Its efficacy was also demonstrated in the treatment of rheumatoid arthritis and inflammatory myositis. The mechanism of B-cell depletion and anti-tumor activity of rituximab is still unclear. Its efficacy could be attributed to apoptosis, complement-dependent cytotoxicity (CDC) and antibody-dependent cellular cytotoxicity (ADCC) (Harris, 2004; Hiddemann et al., 2005a). The specific antigen for rituximab, CD20 is a tetraspan cell surface molecule, which is not internalized in response to antibody binding (Boye et al., 2003; Eisenberg and Looney, 2005). Its restricted expression only in B lymphocytes and absence of expression on bone marrow stem cells represent attractive advantages for targeted therapy. Most efficient rituximab therapy in non-Hodgkin B lymphoma is currently achieved by combination with chemotherapy, such as in CHOP-rituximab treatment (Czuczman et al., 2004; Hiddemann et al., 2005b).

In our laboratory, two different approaches of active tumor targeting have been previously described: (i) direct targeting when PLA NPs were covalently coupled to mAbs and (ii) a pretargeting multistep-method which involves an avidin–biotin system (Nobs et al., 2006). Nobs et al. obtained mAbs modified NPs of around 400 nm. In vivo, these NPs will be preferentially distributed in mononuclear phagocytic system (MPS) rich organs, such as liver and spleen and rapidly eliminated after opsonization (Brigger et al., 2002). Therefore, one of the aims of present work was to decrease the size of NPs in order to have a longer circulation half-live and to increase the chance to reach the target site.

Anti-HER2 (internalizing mAb) and anti-CD20 (non-internalizing mAb) were covalently coupled to the NPs using the direct targeting approach. Assays were also performed to study the influence of different concentrations of –SH groups on the amount of mAbs bound to the NPs. The specific interaction as well as cellular localization of anti-HER2 NPs and anti-CD20 NPs in SKOV-3 and Daudi cells, respectively, were studied by confocal laser scanning microscopy.

2. Material and methods

2.1. Materials

Poly(DL-lactic acid) (100DL 4A, Mw 57 kDa) was provided by Lakeshore Biomaterials, Inc. (Birmingham, AL). 1-Ethyl-3-(3-dimethylaminopropyl)-carbodiimide (EDAC), D(+)-trehalose dihydrate, phosphate buffer saline (PBS), poly-L-lysine solution, 0.1% (w/v) from Sigma (Buchs, Switzerland), *m*-maleimidobenzoyl-*N*-hydroxy-sulfosuccinimide ester (sulfo-MBS), Tris (2-carboxyethyl)-phosphine hydrochloride (TCEP) and D-salt dextran plastic columns were supplied by Pierce (Rockford, IL, USA), Dioctadecyloxacarbo-cyanine perchlorate (DiO) and Concanavalin A AlexaFluor® 594 conjugate were from Molecular Probes (Leiden, The Netherlands). Anti-CD20 (rituximab, Mabthera®) and anti-HER2 (trastuzumab, Herceptin®) were purchased from Roche (Basle, Switzerland). Poly(vinyl alcohol) (Mowiol 4–88) was purchased from Hoechst (Frankfurt/M, Germany).

2.2. Cell lines

The human lymphoma cell line, Daudi and human ovarian carcinoma cells, SKOV-3 (American Type Culture Collection ATCC, Manassas, VA) were grown in RPMI-1640 medium with Glutamax I (Gibco, Grand Island, NY) supplemented with 10% (v/v) fetal calf serum (FCS) (Brunschwig, Basle, Switzerland), penicillin (100 units/ml) and streptomycin (100 μg/ml) (Gibco, Grand Island, NY) at 37 °C in humidified incubator containing 5% CO_2. For all experiments, before incubation with NPs, SKOV-3 cells, maintained in monolayer, were harvested using TrypLE Express (Gibco, Grand Island, NY), whereas Daudi cells, grown in suspension, were centrifuged. In both cases, the cells were resuspended in fresh complete medium for a concentration of about 1×10^6 cells/ml.

2.3. Preparation of PLA NPs

PLA NPs were prepared by a salting-out process as described previously (De Jaeghere et al., 2000). Briefly, 10 g of an aque-

ous solution containing 15% (w/w) poly(vinyl alcohol) (PVAL) and 60% (w/w) magnesium chloride hexahydrate were mixed under vigorous stirring with 4 g of an organic phase containing 18% PLA (w/w) dissolved in acetone. To determine the cellular localization of nanoparticles, DiO 0.01% (w/w) was added in the organic phase as fluorescent probe. The NPs were purified by three successive centrifugations (26,000 × *g* for 40 min). After preparation and purification, the NPs were lyophilized in presence of trehalose as a lyoprotector.

2.4. Thiolation of NPs

Thiol functions were covalently bound to the PLA NPs by a two-step carbodiimide reaction as described earlier (Nobs et al., 2006). Briefly, 100 mg PLA NPs were suspended in 5 ml water and reaction was initiated by adding, consecutively 10 ml of a solution of EDAC (24 mg/ml) and 5 ml of cystamine solution at different concentrations: 2, 4, 10, 32, 71, 120 mg/ml (25, 50, 127, 405, 896, 1518 mol cystamine/mol PLA) to vary the –SH concentration on the particle surface. The final suspension was completed with water to 25 ml and stirred under mild conditions during 24 h at room temperature. Thereafter, EDAC and non-reacted cystamine were removed by three successive centrifugations (25,000 × *g* for 30 min). The NPs were re-suspended in purified water. For reduction of disulfide bonds, the NPs were incubated for 3 h with 1 ml solution of TCEP (6 mg/ml). Finally, the NPs-SH were purified by three successive centrifugations (25,000 × *g* for 30 min) and freeze-dried in presence of trehalose (30%, w/w). The concentration of –SH functions on the surface of nanoparticles was determined spectrophotometrically at λ = 410 nm (Hewlett Packard, Model 8453, Germany) using Ellman's reagent (Nobs et al., 2003). The size of NPs was measured by photon correlation spectroscopy using a Zetasizer 3000 HS (Malvern instruments Ltd., UK).

2.5. Activation of mAb and covalent attachment to the thiolated NPs

The covalent attachment of mAb to the NPs-SH was performed according to a previously described method (Nobs et al., 2006). mAb were purified by size exclusion chromatography using a D-salt desalting column. Two milligrams purified Herceptin® or Mabthera® were activated in PBS (pH 7.4) with sulfo-MBS at a molar ratio 1:20 (mAbs:sulfo-MBS) for 1 h at room temperature. Non-reacted sulfo-MBS was removed by size exclusion chromatography using desalting columns. Five hundred microliters activated anti-HER2 or anti-CD20 mAb (1 mg/ml) were incubated with 500 μl NPs-SH (20 mg/ml) and gently shaken for 60 min at RT. Three batches of NPs-SH have been used with different concentrations of –SH functions: around 200, 300 and 400 mmol-SH/mol PLA. Thereafter, unconjugated mAb were removed by two cycles of centrifugation (25,000 × *g*, 10 min). The amount of mAb conjugated to NP was determined indirectly by measuring uncoupled mAb in the supernatant after centrifugation step. A spectrophotometric method (λ = 280 nm) (Hewlett Packard, Model 8453, Germany) was used assuming an extinction coefficient of 1.4 M^{-1} cm^{-1}. Finally, mAb-NPs were stored in PBS at 4 °C. In order to verify the efficacy of mAb-conjugation to NPs, selected experiments were also performed using trace amounts of ^{125}I radiolabeled rituximab mixed with native antibodies. Antibody radiolabeling was performed using the chloramin T method with minor modifications as described (Schaffland et al., 2004). Briefly, 0.1 ml clinical grade rituximab (1 mg) solution and 100 μl freshly prepared chloramine T solution (0.5 mg per 1 ml, in sterile phosphate buffer 0.15 M, pH 7) were reacted with 37 MBq $Na^{125}I$ solutions, previously diluted to 200 μl with 0.15 M phosphate buffer pH 7.0, for 5 min at room temperature. The solution of labeling antibodies was purified through a 2 ml reversible column (Supelco, Buchs, Switzerland) filled with 1.8 g of anion exchange resin (Dowex 1 × 8, 100 mesh) at 0.5 ml/min flow. The labeling vial was washed with 2 ml 0.9% NaCl solution that was also passed through the resin filter. Furthermore, 3 kBq of radiolabeling mAbs (10 μl) were added to 2 ml purified rituximab (5 mg/ml). The rituximab solution containing a trace amount of ^{125}I-labeled mAbs was used for coupling reaction. The percentage of rituximab bound to the NPs-SH was determined by direct radioactivity counting of mAb-NPs in comparison with the input radioactivity (100%). The number of mAbs molecules bound on the surface of a single nanoparticle was calculated using the following equation (Nobs et al., 2004b):

$$n = aN\left(\frac{d4}{3\pi r^3}\right)$$

where n is the number of mAbs per nanoparticle, a the mol of mAbs per g PLA, d the density of nanoparticles estimated to be 1.5 g/cm^3 based on the polymer density, r the mean radius of nanoparticles and N is the 6.022×10^{23} (Avogadro Number).

A control was performed using PLA NPs (without –SH groups) to determine the fraction of non-covalently attached mAb on the surface of the NPs.

2.6. Cellular localization of anti-HER2 NPs and anti-CD20 NPs

Cellular distribution experiments were performed using Daudi cells expressing CD20 antigen (negative for HER2) and SKOV-3 cells overexpressing HER2 antigen (negative for CD20). Approximately, 1×10^6 SKOV-3 or Daudi cells were incubated with 100 μl (1 mg/ml) suspension of mAbs-NPs, in fresh culture medium for different times (1 and 6 h) at 37 °C. To analyze non-specific interaction between cells and nanoparticles, controls were performed using unmodified NPs and modified NPs with a non-specific mAb. After incubation, the cells were rinsed twice with cold PBS. The cell membranes were stained for 3 min with a solution of Concanavalin A AlexaFlour 594 in PBS (0.05% w/v). After two washing steps with cold PBS, the cells were fixed with paraformaldehyde 4% (v/v) for 30 min. The paraformaldehyde was removed by three washings with PBS. The cells were fixed on the slides with poly-L-lysine solution and covered with coverslips. The slides were observed using a confocal laser scanning microscope, LSM 510 META (Zeiss AG, Zurich, Switzerland) equipped with argon and helium/neon lasers. Two channels at 488 and 543 nm laser excitation were

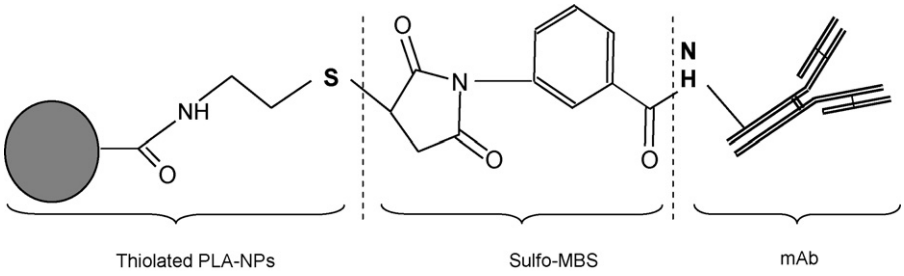

Fig. 1. Schematic representation of antibody modified nanoparticles (not to scale).

chosen. A Zeiss Plan-Apochromat 63×/1.4 oil objective was used. A Z Stack of images was displayed in an orthogonal view using LSM 510 META software.

3. Results

Antibody coupling to NPs was performed in two steps: introduction of –SH groups on the surface of PLA NPs and covalent coupling of antibodies to NPs-SH via the bifunctional cross-linker, sulfo-MBS (Fig. 1).

3.1. Thiolation of NPs

PLA NPs with free carboxylic functions were prepared by a salting-out method. We selected a high concentration of PVAL (15%, w/w) in aqueous solution, which allowed obtaining small NPs with a mean size of about 170 ± 13 nm.

The influence of cystamine concentration on the amount of –SH introduced on the NPs surface has been studied. With increasing concentrations of cystamine the amount of –SH functions increased and tended, however, to reach saturation at the higher concentrations (Fig. 2). The maximum concentration of –SH groups was about 400 mmol-SH/mol PLA. This corresponds to about 25,000 –SH groups per NP. For further experiments, three concentrations of cystamine were used: 25, 127, 896 mol cystamine/mol PLA. These concentrations resulted in the introduction of a mean of 217 ± 30, 295 ± 27 and 385 ± 35 mmol-SH/mol PLA, respectively, in different experiments.

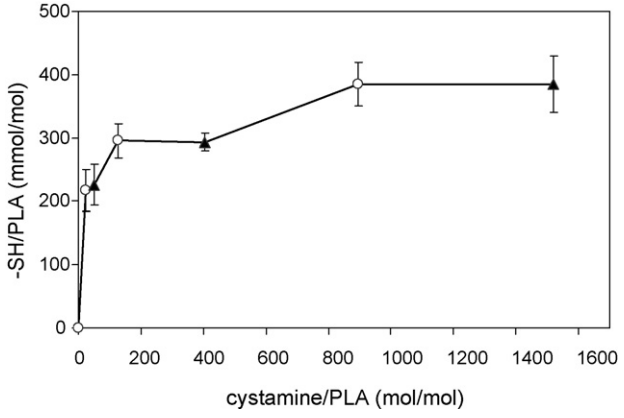

Fig. 2. Variation of thiol concentration on NPs surface as a function of cystamine concentration. (▲) Points used for further experiments. Mean ± S.D. ($n > 3$).

The nanoparticle size increased from an initial size of 170 ± 13 to 202 ± 15 nm after maximal thiolation.

3.2. Covalent coupling of mAb to the thiolated NPs

The influence of –SH concentration on the amount of mAb coupled to the NPs was studied using three batches of NPs-SH with different thiol concentrations of about 200, 300, 400 mmol-SH/mol PLA. Evaluating constant concentrations of activated mAb with the different batches of NPs-SH, the amount of mAb coupled to the NPs after 1 h at RT was not influenced by the concentration of –SH functions, both for rituximab and trastuzumab. The controls performed with activated anti-CD20 and non-thiolated NPs showed that only a minor quantity of mAb (0.7 mmol anti-CD20/mol PLA) was non-specifically attached to the NPs.

In order to verify the efficacy of mAb-conjugation to NPs, selected experiments were also performed using trace amounts of radiolabeled antibody mixed with native antibodies. These experiments allowed the calculation of the percentage of mAb coupling by direct radioactivity counting of mAb-NPs in comparison with the input radioactivity (100%). A good correlation of results of the optical density measurements, described above, and direct radioactivity counting of mAb-NPs was observed (results not shown).

The amount of mAb conjugated to NPs-SH was in the range of 3 mmol anti-HER2/mg NPs and 5 mmol anti-CD20/mol PLA for the selected condition of incubation of 50 μg antibody/mg NPs-SH. These results translate to approximately 295 anti-HER2 and 557 anti-CD20 molecules, respectively, per NP. Antibody coupling efficiency was about 16% and 25% for anti-HER2 and anti-CD20 mAbs, respectively. Fig. 3 shows a representative experiment of anti-CD20 coupling. After antibody coupling, the size of both nanoparticle formulations was very similar, about 250 nm (Table 1).

Table 1
Physico-chemical characteristics of anti-HER2 and anti-CD20 modified NPs

Parameter	Anti-HER2 NPs	Anti-CD20 NPs
Particle size (nm)	264 ± 5	256 ± 25
Polydispersity index (P.I.)	0.2	0.1
Concentration of mAbs (μg mAb/mg NPs)	8	14
Number of antibody/NP	295	557
Efficiency of mAb coupling (%)	16	25

P.I.: Scale from 0 to 1.

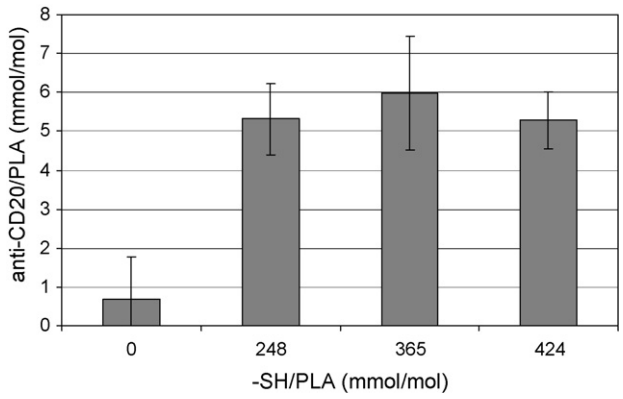

Fig. 3. Influence of thiol functions on the amount of anti-CD20 bound to the NPs. Control (0) was performed using non-thiolated NPs incubated with activated anti-CD20 mAb.

3.3. Tumor cell interaction with mAb coupled-NPs

The targeting of SKOV-3 and Daudi cells with anti-HER2 NPs and anti-CD20 NPs, respectively, demonstrated for both formulations a strong interaction between cells and NPs modified with the relevant mAb (Fig. 4A and E). Control nanoparticles either lacking antibodies or coupled with the non-relevant antibodies showed a very minor non-specific interaction with SKOV-3 (Fig. 4B and C) and Daudi cells (Fig. 4D and F). These results demonstrate the preserved immunoreactivity of the mAb-NPs and the specific interaction of the mAb-NPs with the respective target cells.

3.4. Subcellular localization of mAb coupled-NPs

Confocal microscopy showed two different cellular localizations of mAb-NPs (Fig. 5). *xy* section views were combined with *xz*/*yz* sections for a better visualization of NPs distribution.

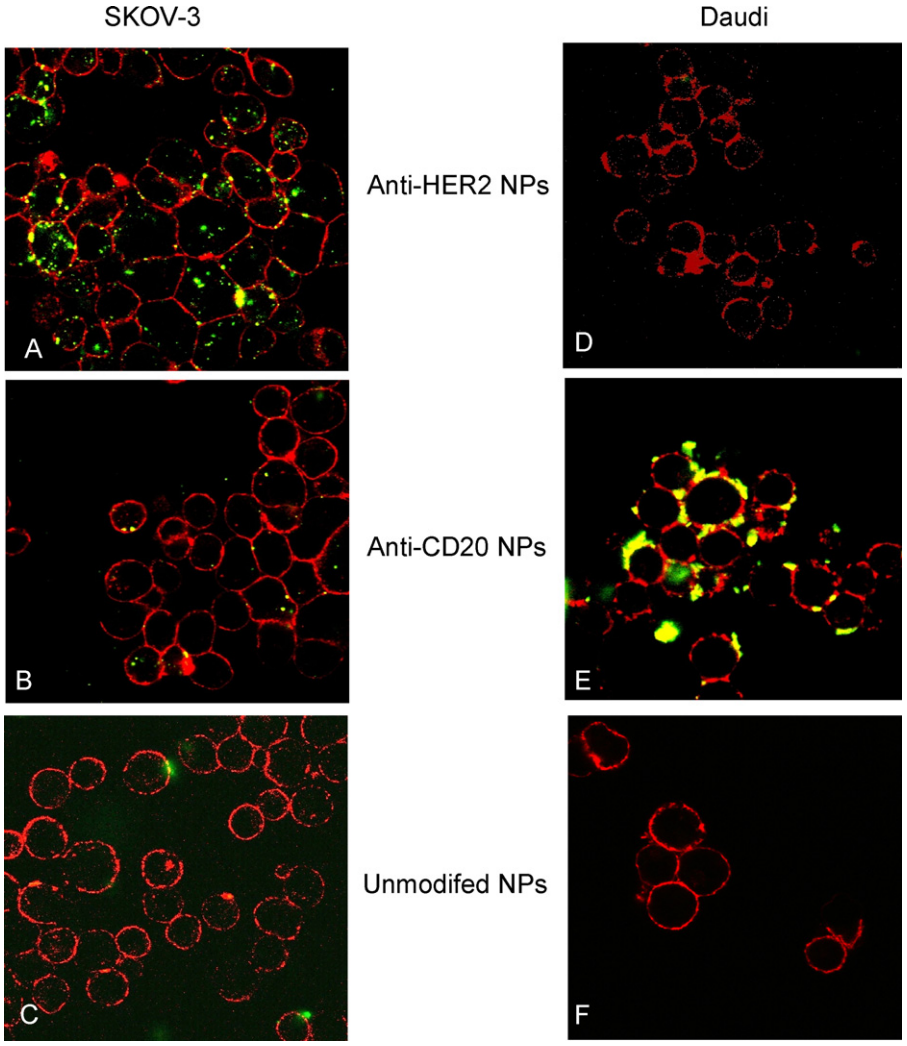

Fig. 4. Specific interaction of mAb-NPs in SKOV-3 and Daudi cells studied by confocal laser scanning microscopy (objectif: 63×). Cell membranes were stained in red with Concanavalin A AlexaFluor® 594 conjugate, whereas NPs were stained in green with DiO. The cells were incubated with 1 mg/ml mAb labeled NPs or non-conjugated NPs at 37 °C for 6 h. (A and D) Anti-HER2 NPs; (B and E) anti-CD20 NPs; (C and F) unmodified NPs. *Note*: In (A) the clear distinction of red membranes and green anti-HER2 NPs, since the latter are internalized and therefore dissociated from the cell membrane, while in (E) the binding of anti-CD20 NPs to the cell membrane leads to the superposition of green and red fluorescence and appearance in yellow.

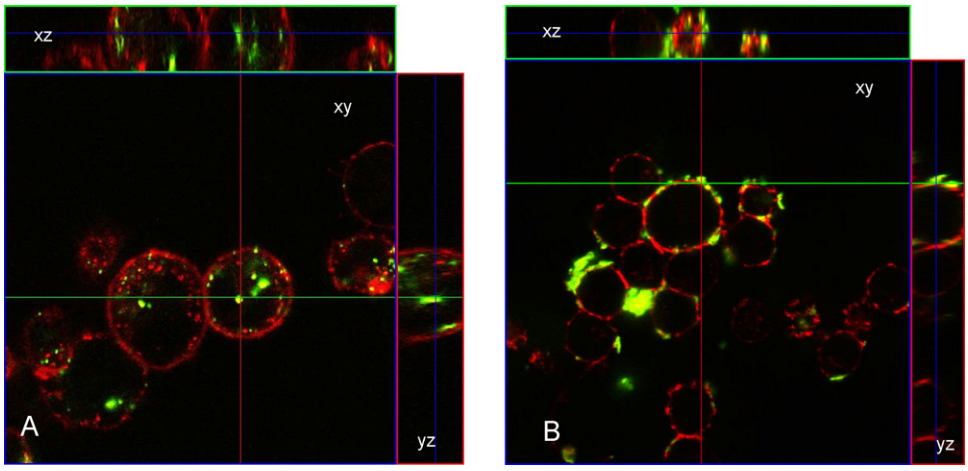

Fig. 5. Orthogonal views of (A) anti-HER2 NPs incubated with SKOV-3 cells and of (B) anti-CD20 NPs incubated with Daudi cells. In center: *xy* section, on the top: *xz* section and on the right: *yz* section.

In case of SKOV-3 cells, the internalization of the anti-HER2 NPs was observed whereas for Daudi cells, the anti-CD20 NPs remained localized on the cellular surface (Fig. 5A and B) after 1 h of incubation at 37 °C. For anti-HER2 NPs, their intracellular uptake increased after 6 h of incubation at 37 °C compared with 1 h incubation (data not shown). Extension of the incubation time to 6 h increased the surface accumulation of anti-CD20 NPs on Daudi cells but still without internalization.

4. Discussion

Active drug targeting represents a promising approach for treatment of cancer when specific expression of particular target antigens, receptors and biomarkers can be exploited. This condition is fulfilled with the two mAbs used here as shown by multiple clinical studies. For rituximab, the CD20 antigen expression is restricted to normal B-cells and B-cell lymphoma while absent of T lymphocytes and bone marrow stem cells. During rituximab treatment, T cell immunity is therefore not affected and repopulation of the normal B-cell repertoire after treatment termination remains guaranteed by the preserved stem cells. With respect to trastuzumab, normal cells can express moderate amounts of HER2 target antigen while tumors of certain patients overexpress this antigen. It appears that this difference between healthy tissues and tumors allows the efficient application of this antibody in patients.

The concept of active targeting may be achieved by covalent or non-covalent binding of nanocarrier systems to a tumor recognition moiety, which ensures the specific distribution of drug into targeted tissue (Nobs et al., 2004a). Direct conjugation of a drug molecule with a homing moiety is also possible (Jaracz et al., 2005) but drug carrier systems have clear advantages, such as high drug loading capacity, possibility to control their size and drug activity is not affected by coupling reactions.

Two types of antibody modified nanoparticles, anti-HER2 NPs and anti-CD20 NPs, were prepared in the present work by covalent attachment of the mAb via a thioester linkage with NPs.

One of the aims of this study was to develop small NPs. Decreasing the size of NPs might improve their ability to extravasate into target tissues and to avoid phagocytic uptake (Brigger et al., 2002). Indeed, we managed to obtain antibody coupled nanoparticles of about 250 nm while in previous studies the size of mAb modified nanoparticles were in the range of 340–410 nm (Nobs et al., 2006).

Also, we showed that the number of –SH groups on the NPs surface can be modulated using different concentrations of cystamine. However, the –SH concentration at the NPs surface had no influence on the amount of mAb bound. It is possible that steric hindrance of antibodies might limit the number of molecules coupled to the surface of each nanoparticle.

The coupling efficiency of antibody could influence cellular interaction of nanocarrier systems. In a previous work, the highest amount of antibody on the NP surface (approximately 2500 mAbs molecules per NPs) showed the lowest cellular binding probably due to an inactivation of antibody (Nobs et al., 2006). Kirpotin et al. reported that internalization efficacy of anti-HER2 immunoliposomes increased with the increase in surface density of conjugated Fab fragments before reaching a plateau at 15 Fab/liposome (Kirpotin et al., 1997). These results suggest that an optimal number of ligands would be necessary to achieve efficient cellular targeting of anti-HER2 nanocarriers. In our study, approximately 295 and 557 molecules of anti-HER2 and anti-CD20 antibodies, respectively, were bound to NPs-SH. Similar results were obtained in other studies using human serum albumin modified NPs, when 429 molecules of trastuzumab were bound per NP (Steinhauser et al., 2006).

The two mAbs used in this study present different mechanisms of interaction with tumor cells: the CD20 antigen is known not to become internalized upon antibody binding whereas the HER2 antigen is internalized. An efficient internalization of anti-HER2 NPs could indeed be observed in SKOV-3 cells overexpressing HER2 (Fig. 4). These results are in line with other studies demonstrating specific binding and internalization of anti-HER2 nanoparticulate drug delivery systems, such as immunoliposomes or immunonanoparticles (Kirpotin et al., 1997; Wartlick et al., 2004). Also, therapeutic efficiency of anti-HER2 immunoliposomes-doxorubicine was shown in a tumor xenograft model (Park et al., 2002).

In contrast to anti-HER2 NPs, the anti-CD20 NPs were not internalized. Despite the fact that multiple antibodies per NP can react with cells, internalization could not be observed with the anti-CD20 NPs even after prolonged incubation. The proposed mechanism of interaction between Daudi and anti-CD20 NPs is a cell surface clustering (Shan et al., 1998).

Non-internalizing NPs remain of interest as anti-tumor drug carriers for at least two reasons: first, the drug released on the cell surface can be taken up by passive diffusion or another mechanism via endocytic pathways including clathrin-coated pits, caveole membrane invaginations, phagocytosis and pinocytosis phenomenons (Rejman et al., 2004; Koo et al., 2005). Secondly, the observation of direct induction of apoptosis by cross-linked anti-CD20 antibodies (Shan et al., 1998) might provide additional efficacy to anti-CD20 NPs by the fact that the multiple antibodies per NP might represent a new efficient method of cross-linking.

5. Conclusion

The efficiency of mAb modified NPs in specific tumor cell targeting was demonstrated in vitro. Furthermore, confocal microscopy showed a different cellular localization of NPs depending on the type of antibody–antigen interaction involved. These two model situations will allow evaluating in a next step the efficiency of the mAb-NPs as carrier of cytostatic drugs. Finally, different in vivo tumor models are available for these two mAb-NPs conjugates that will allow testing of their efficiency in specific tumor targeting.

References

Boye, J., Elter, T., Engert, A., 2003. An overview of the current clinical use of the anti-CD20 monoclonal antibody rituximab. ESMO 14, 520–535.

Brigger, I., Dubernet, C., Couvreur, P., 2002. Nanoparticles in cancer therapy and diagnosis. Adv. Drug Deliv. Rev. 54, 631–651.

Czuczman, M.S., Weaver, R., Alkuzweny, B., Berlfein, J., Grillo-Lopez, A.J., 2004. Prolonged clinical and molecular remission in patients with low-grade or follicular non-Hodgkin's lymphoma treated with rituximab plus CHOP chemotherapy: 9-year follow-up. J. Clin. Oncol. 22, 4711–4716.

De Jaeghere, F., Allemann, E., Feijen, J., Kissel, T., Doelker, E., Gurny, R., 2000. Freeze-drying and lyopreservation of diblock and triblock poly(lactic acid)–poly(ethylene oxide) (PLA–PEO) copolymer nanoparticles. Pharm. Dev. Technol. 5, 473–483.

Duncan, R., 1999. Polymer conjugates for tumor targeting and intracytoplasmic delivery. The EPR effect as a common gateway? Pharm. Sci. Technol. Today 2, 441–449.

Eisenberg, R., Looney, R.J., 2005. The therapeutic potential of anti-CD20. Clin. Immunol. 117, 207–213.

Harries, M., Smith, I., 2002. The development and clinical use of trastuzumab (Herceptin). Endocr. Relat. Cancer 9, 75–85.

Harris, M., 2004. Monoclonal antibodies as therapeutic agents for cancer. Lancet Oncol. 5, 292–302.

Hiddemann, W., Buske, C., Dreyling, M., Weigert, O., Lenz, G., Forstpointner, R., Nickenig, C., Unterhalt, M., 2005a. Treatment strategies in follicular lymphomas: current status and future perspectives. J. Clin. Oncol. 23, 6394–6399.

Hiddemann, W., Kneba, M., Dreyling, M., Schmitz, N., Lengfelder, E., Schmits, R., Reiser, M., Metzner, B., Harder, H., Hegewisch-Becker, S., Fischer, T., Kropff, M., Reis, H.E., Freund, M., Wormann, B., Fuchs, R., Planker, M., Schimke, J., Eimermacher, H., Trumper, L., Aldaoud, A., Parwaresch, R., Unterhalt, M., 2005b. Frontline therapy with rituximab added to the combination of cyclophosphamide, doxorubicin, vincristine, and prednisone (CHOP) significantly improves the outcome for patients with advanced-stage follicular lymphoma compared with therapy with CHOP alone: results of a prospective randomized study of the German Low-Grade Lymphoma Study Group. Blood 106, 3725–3732.

Ignatius, A.A., Claes, L.E., 1996. In vitro biocompatibility of bioresorbable polymers: poly(L,DL-lactide) and poly(L-lactide-coglycolide). Biomaterials 17, 831–839.

Jaracz, S., Kuznetsova, L.V., Ojima, I., 2005. Recent advances in tumor-targeting anticancer drug conjugates. Bioorg. Med. Chem. 13, 5043–5054.

Kirpotin, D., Park, J.W., Hong, K., Zalipsky, S., Li, W.L., Carter, P., Benz, C.C., Papahadjopoulos, D., 1997. Sterically stabilized anti-HER2 immunoliposomes: design and targeting to human breast cancer cells in vitro. Biochemistry 36, 66–75.

Koo, O.M., Rubinstein, I., Onyuksel, H., 2005. Role of nanotechnology in targeted drug delivery and imaging: a concise review. Nanomedicine 1, 193–212.

Lukyanov, A.N., Elbayoumi, T.A., Chakilam, A.R., Torchilin, V.P., 2004. Tumor-targeted liposomes: doxorubicin-loaded long-circulating liposomes modified with anti-cancer antibody. J. Control. Release 100, 135–144.

Maeda, H., 2001. The enhanced permeability and retention (EPR) effect in tumor vasculature: the key role of tumor-selective macromolecular drug targeting. Adv. Enzyme Regul. 41, 189–207.

Nahta, R., Esteva, F.J., 2006. Herceptin: mechanisms of action and resistance. Cancer Lett. 232, 123–138.

Nobs, L., Buchegger, F., Gurny, R., Allemann, E., 2003. Surface modification of poly(lactic acid) nanoparticles by covalent attachment of thiol groups by means of three methods. Int. J. Pharm. 250, 327–337.

Nobs, L., Buchegger, F., Gurny, R., Allemann, E., 2004a. Current methods for attaching targeting ligands to liposomes and nanoparticles. J. Pharm. Sci. 93, 1980–1992.

Nobs, L., Buchegger, F., Gurny, R., Allemann, E., 2004b. Poly(lactic acid) nanoparticles labeled with biologically active Neutravidin for active targeting. Eur. J. Pharm. Biopharm. 58, 483–490.

Nobs, L., Buchegger, F., Gurny, R., Allemann, E., 2006. Biodegradable nanoparticles for direct or two-step tumor immunotargeting. Bioconjug. Chem. 17, 139–145.

Panyam, J., Labhasetwar, V., 2003. Biodegradable nanoparticles for drug and gene delivery to cells and tissue. Adv. Drug Deliv. Rev. 55, 329–347.

Park, J.W., Hong, K., Kirpotin, D.B., Meyer, O., Papahadjopoulos, D., Benz, C.C., 1997. Anti-HER2 immunoliposomes for targeted therapy of human tumors. Cancer Lett. 118, 153–160.

Park, J.W., Hong, K., Kirpotin, D.B., Colbern, G., Shalaby, R., Baselga, J., Shao, Y., Nielsen, U.B., Marks, J.D., Moore, D., Papahadjopoulos, D., Benz, C.C., 2002. Anti-HER2 immunoliposomes: enhanced efficacy attributable to targeted delivery. Clin. Cancer Res. 8, 1172–1181.

Rejman, J., Oberle, V., Zuhorn, I.S., Hoekstra, D., 2004. Size-dependent internalization of particles via the pathways of clathrin- and caveolae-mediated endocytosis. Biochem. J. 377, 159–169.

Sapra, P., Allen, T.M., 2003. Ligand-targeted liposomal anticancer drugs. Prog. Lipid Res. 42, 439–462.

Schaffland, A.O., Buchegger, F., Kosinski, M., Antonescu, C., Paschoud, C., Grannavel, C., Pellikka, R., Delaloye, A.B., 2004. ^{131}I-rituximab: relationship between immunoreactivity and specific activity. J. Nucl. Med. 45, 1784–1790.

Shan, D., Ledbetter, J.A., Press, O.W., 1998. Apoptosis of malignant human B cells by ligation of CD20 with monoclonal antibodies. Blood 91, 1644–1652.

Steinhauser, I., Spaenkuch, B., Strebhardt, K., Langer, K., 2006. Trastuzumab-modified nanoparticles: optimisation of preparation and uptake in cancer cells. Biomaterials 27, 4975–4983.

Wartlick, H., Michaelis, K., Balthasar, S., Strebhardt, K., Kreuter, J., Langer, K., 2004. Highly specific HER2-mediated cellular uptake of antibody-modified nanoparticles in tumour cells. J. Drug Target. 12, 461–471.